Polymer Testing xxx (xxxx) xxxx

Contents lists available at ScienceDirect

Polymer Testing

journal homepage: www.elsevier.com/locate/polytest

Material Characterisation

Characterization of interlaminar fracture modes I, II, and I-II of carbon/epoxy composites including in-service related bonding quality conditions

Masoud Yekani Fard[a,*], Brian Raji[b], John Woodward[a], Aditi Chattopadhyay[a]

[a] School for Engineering of Matter, Transport and Energy, Arizona State University, Arizona, USA
[b] Pipe Reconstruction Inc, 2800 North Central Avenue, Phoenix, AZ, 85004, USA

ARTICLE INFO

Keywords:
A. Polymer matrix composites (PMCs)
B. Fracture
C. Degradation
D. Testing
E. Heat
F. Humidity

ABSTRACT

The effects of hot/wet environmental conditions for intervals of one and two years of exposure on fracture modes I, II, and I-II of biaxial carbon/epoxy composites were characterized. Tests were carried out on double cantilever beam, end-notched flexure, four-point end-notched flexure, and mixed mode bending specimens. For the purposes of this study, it was recognized that water absorption was governed by the Fickian mechanism. The effective crack method was used to analyze mode II and mode I-II with a high shear mode participation ratio. Hygrothermal effects degraded initiation toughness in all fracture modes, and extensive fiber bridging along with multiple damage modes within the mid-layers in specimens exposed to heat and humidity altered crack propagation behavior. Mixed mode fracture test results revealed a weak interaction between modes I and II for most parts of G_I/G_{II}, but the interaction was strongest when the fracture behavior changed from a pure mode to a mixed mode condition.

1. Introduction

Catastrophic failure due to delamination during service life is one of the major obstacles preventing the full utilization of composite materials and their full mechanical potential, particularly in industry applications. Most literature on interlaminar fracture toughness has been limited by less-than-optimal curing conditions and uncontrollable laboratory parameters. Delamination in a real-world structure under realistic loading and environmental conditions often manifests as a mixed-mode fracture. Investigations pertaining solely to one mode of fracture are valuable, but they do not provide the requisite amount of information needed to precisely understand and design critical structures for their intended life span. While the ASTM standard recommends the double cantilever beam (DCB) method and has focused on smooth quasi-static crack growth for mode I fractures, several studies have reported both smooth and non-smooth crack growth in a quasi-static range [1–5]. Even for the same type of material and same loading rate, no consistent observations have been reported [2,3].

Researchers have used a multitude of test methods to study mode II fracture [5–11]. End-notched flexure (ENF) [6,9], four-point end-notched flexure (4ENF) [7,10], and end loaded split (ELS) [6,9] have all been utilized to characterize in-plane shear fracture. The majority of studies in the reviewed literature found that the 4ENF test protocol produced up to 20% higher fracture properties than the ENF test protocol. This difference is mainly attributable to the effects of geometry, nonlinearity, friction, and fixture compliance. The mixed mode bending (MMB) test proposed by Reeder and Crews [12,13] was used to study mixed mode I-II fractures.

Quasi-static crack growth is defined as equilibrium between the driving force for crack propagation and the total dissipated energy. Dynamic crack growth, corresponding to a load drop or a jump in the crack length within the system, can occur when the elastic energy stored within the system is sufficient to initiate crack growth, with no additional work required to be performed on the mechanical system. This can be ascribed to local instabilities in a quasi-static system and is referred to as stick-slip behavior. Kusaka et al. [2] and Davidson and Waas [3] observed both unstable and stable crack growth. Non-smooth crack growth and significant fiber bridging in carbon fiber composites was observed at the loading rate around 0.01 mms^{-1} by Kusaka et al. [2] and Morais and Pereira [11].

Schuecker and Davidson [7] demonstrated that the effect of friction on G_{IIc} is slightly higher for 4ENF than ENF. Improved 4ENF results were shown using linear variable differential transducers beneath the loading pins in other studies [8,10]. One major issue in mode II testing is error in measuring crack length during the testing. Locating the crack tip is extremely inconsistent due to the existence of the fracture process zone (FPZ) and the contact between cracked faces [11]. The effective crack method (ECM) has been recognized as a powerful technique to

* Corresponding author.
E-mail address: Masoud.yekanifard@asu.edu (M.Y. Fard).

https://doi.org/10.1016/j.polymertesting.2019.05.010
Received 25 March 2019; Received in revised form 2 May 2019; Accepted 8 May 2019

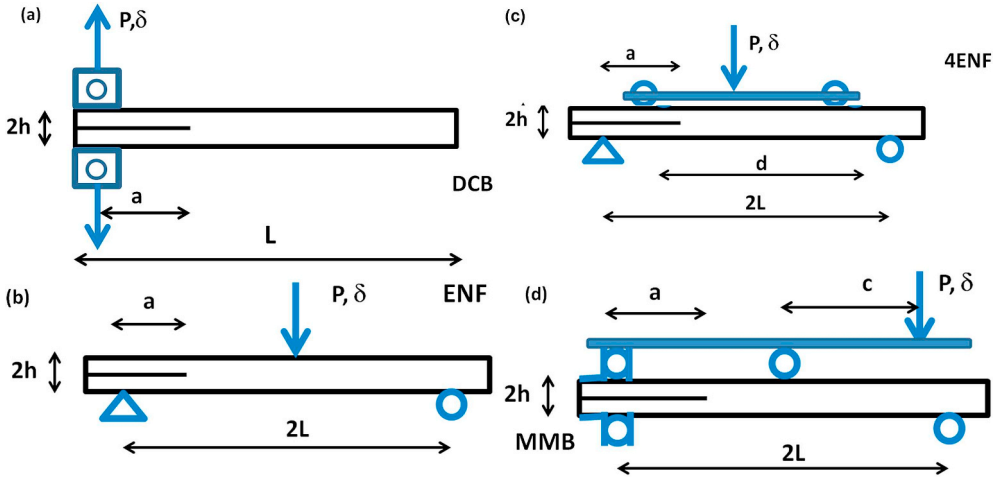

Fig. 1. DCB, ENF, 4ENF, and MMB fracture test configuration. (For interpretation of the references to color in this figure legend, the reader is referred to the Web version of this article.)

locate the crack tip for governing in-plane shear ENF and ELS fracture, despite the complexities inherent in unstable crack propagation during testing. Applying ECM to determine the mode I fracture was not successful due to fiber bridging behind the crack tip. Several empirical equations such as the super ellipse stress intensity factor, linear equation, nonlinear failure locus have been suggested for crack initiation criteria for mode I-II [12–21]. A higher mode I critical stress intensity factor was observed at the very low ratio of in-plane shear stress to normal stress [16]. These observations were obtained using laboratory specimens under laboratory conditions.

The effect of temperature change on fracture properties in a single mode has received attention in recent years [22–29]. Researchers observed either an increase or no change in critical strain energy release rates with greater temperatures below the glass transition temperature [22,23]. Adhesive failure and alternating crack path type behavior were observed in thermal and moisture degraded specimens, respectively, by Markatos et al. [22]. Effects of 'free' water and 'bound' water on fracture properties of composite joints have additionally been studied by researchers [24–29]. 'Free' water disrupts the Van der Waals forces and increases the chain segment mobility while 'bound' water forms multiple hydrogen bonds [25]. Mohan et al. [24] observed that only 'free' water would affect the glass transition temperature (T_g) of some adhesives while for some others both 'free' and 'bound' water may affect T_g. 'Free' water can reduce T_g while 'bound' water can exhibit the opposite effect. Reeder [16] (for AS4/3501 carbon/epoxy laminates), Benzeggagh and Kenane [21] (for glass fiber), Mohan et al. [24,25] (for unidirectional carbon fiber/epoxy prepreg), and Hooper and Subramanian [30] (for Fiberite HYE1337AU graphite/epoxy) showed an increase in mode I and II fracture energy due to saturation. Hooper et al. [30] observed more broken fibers and more fibers covered with epoxy resin in saturated specimens. No specific reason was provided by the authors as an explanation for the increase in initiation fracture energy in saturated specimens. Belec et al. [31] studied the effects of natural and artificial aging conditions on the interphase of epoxy and carbon fiber at nanoscale. They found that the hygrothermal conditions (70 °C and 85% RH) softens the interphase mainly during the first 6 weeks of exposure, and subsequently observed a dramatic reduction in T_g at up to 5 months and a much lower rate of reduction up to 20 months of exposure to hot/wet conditions (70 °C and 85% RH). The study conducted by Alessi et al. [32] showed that propagation energy release rate in polymer matrix composites increases with water uptake at 70 °C. Alessi [32] also observed smooth load vs. crack opening displacement behavior in high modulus polymer carbon fiber composite conditioned for 8 weeks at 70 °C.

The presented discrepancies between the studies conducted previously can likely be attributed to differences in the manufacturing procedures of the composite laminates and the effects of pre-existing damage. A review of the literature on the fracture properties of PMCs published since 1985 shows that (i) in the case of laboratory fracture properties, there exists some discrepancies among test types, data reduction techniques, and mode interaction and (ii) there is a lack of data on the effects of durability for all modes of fracture. In this study, DCB, ENF (in some cases 4ENF), and MMB experiments were used to investigate mode I, II, and modes I-II, respectively. 60 °C and 90% relative humidity (RH) with exposure intervals of one and two years were used to study the effects of hot/wet environmental conditions on fracture properties. In order to avoid errors in deflection measurement due to the compliance of the fixture and loading frame, digital image correlation (DIC) was used. The effective crack method (ECM) was used to calculate the effective crack length to minimize the errors in crack length measurement during the mode II and for a selection of the mode I-II tests. Although existing studies [9,11] have reported that a suitable approach for mode II characterization is using an ENF specimen with a careful geometry selection (depending on the type of the composite, fabric type, and epoxy toughness) in conjunction with a rigid fixture and combining the two with ECM, 4ENF was still used to further validate initiation toughness. The fracture toughness values obtained from pure and mixed modes were used to develop failure loci for laboratory and conditioned samples with the previously specified exposure intervals.

2. Experiment and specimen configurations

Thick, stitch-bonded biaxial carbon fabric with 24 K and 12 K carbon fiber yarn were used in 0° and 90° orientations, respectively. Epoxy resin bisphenol-A and bisphenol-F type and an amine hardener at a 100:22 mix ratio was used. Several composite panels (350 mm × 350 mm) with 6 stitched plies $[(90/0_2/90_2/0)]_s$ were fabricated on a hot press. The average fabricated laminate thickness was 8.0 mm. A 0.013 mm Teflon film was inserted at the mid-plane in order to create an induced delamination surface. For complete curing, the plates were subjected to 2 MPa in out-of-plane compression at 60 °C for a duration of 8 h. The general configuration and dimensions of DCB, ENF, 4ENF, and MMB specimens are shown in Fig. 1 and Table 1. In this table, a is the delamination length, $2L$ is the span of the structure (L in the case of DCB), d is the distance between loading noses in 4 PB setup, c is the distance to the load application point in MMB, h is the thickness of the delaminated section, and b is the width of the specimen.

All the samples were sectioned with a diamond water saw, with the edges being finished using coarse 300 grit and fine 1500 grit sandpaper.

Table 1
Averaged specimen dimensions (mm).

Type	2 h	a	L	2L	d	c	b
DCB	8.2	55	135	–	–	–	20
ENF	8.0	30	–	100	–	–	20
4ENF	8.0	64	–	160	60	–	20
MMB	8.0	36	–	100	–	32,50,84	20

Table 2
Averaged lamina properties (MPa).

	E_{11}	E_{22}	G_{13}
laboratory	85000	52000	8500
hot/wet conditioned 1 year	80000	32000	5000
hot/wet conditioned 2 year	78000	30000	4900

Environmental conditioning was carried out at 90% RH and 60 °C for the period of one and two years; the specimens maintained at this condition are referred to as "hot/wet" specimens. The specimens kept in desiccators in the laboratory until shortly before testing are referred to as "laboratory" specimens. All the tests were conducted in the laboratory condition. In one of our previously conducted studies, the mechanical properties of the degraded laminates were obtained; the summarization of these results is available in Table 2. All fracture modes were conducted in displacement control mode at a loading rate of 0.5 mm/min. A high magnification camera (model SONY xcd-sx910uv) on one side of the frame was connected to a display to locate and track the delamination tip with a framing rate of 1 Hz. The camera, time synchronized with loading, was used to obtain crack length versus load point displacement. The DIC system (GOM ARAMIS 5 M with 5 mega pixels and strain accuracy up to 100 μstr) situated at the opposite side of the frame was set to monitor crack initiation/propagation. DIC side edges of the specimens were marked at every 1 mm interval by a black pen. A minimum of seven specimens were tested for each series of tests to properly validate the results. The glass transition temperature of dry material (T_{g0}) has been determined as 89 °C ± 2 °C through Dynamic Mechanical Analysis using a DMA Q800 universal V4.5A TA instrument. The test was conducted with a heating rate of 1 °C/min. Scanning Electron Microscopy (SEM) was performed on the fracture surfaces using a XL30 ESEM-FEG. The samples were sputter coated with an approximately 20 nm thick layer of gold prior to high voltage (10 KV) imaging to avoid charging.

3. Moisture diffusion

A Moisture diffusion study was performed as the water absorption percentage from experimental data was only available for certain intervals within the span of 2 years. The model of the moisture distribution demonstrated the change in the water absorption percentage through the cross section for 2 years of constant exposure. Fick's second law of moisture distribution was used to find the weight percent moisture (M) that is linearly related to the total amount of moisture over the entire specimen [33].

$$\frac{M}{M_m} = 1 - \frac{8}{\pi^2}\sum_{j=0}^{\infty}\frac{exp\left[-(2j+1)^2\pi^2\left(\frac{D_{th}\,t}{h^2}\right)\right]}{(2j+1)^2} \tag{1}$$

where M_m is the weight percent moisture at fully saturated condition, h is thickness, t is time and D_{th} is the mass diffusivity along the thickness which is a thermally activated process. D_{th} is related to temperature by the Arrhenius relationship for polymer matrix composites [34–36].

$$D_{th} = 6.51\,exp\left(\frac{-5722}{T}\right) \tag{2}$$

where T is absolute temperature. The local moisture content through the thickness for different ages of exposure if 1D Fickian diffusion governs the moisture absorption mechanisms is as below.

$$\frac{c}{c_m} = 1 - \frac{4}{\pi}\sum_{j=0}^{\infty}\frac{1}{(2j+1)}sin\frac{(2j+1)\pi z}{h}\,exp\left[\frac{-(2j+1)^2\,\pi^2\,D_{th}\,t}{h^2}\right] \tag{3}$$

where c is the local moisture concentration at location z through the thickness at time t and c_m is the moisture concentration at the surface of the composite.

4. Fracture modes

The load corresponding to the onset of visually (from the high magnification camera) recognizable crack growth was used to calculate the critical energy release rate for all fracture modes. Point "Vis." was selected as opposed to points "NL" and "Max", as (i) laboratory and conditioned specimens exhibited different load deflection behaviors in different fracture modes, making a direct comparison of toughness calculated based on "NL" and "Max" difficult to conduct. Conversely, (ii) "Vis." corresponds to crack initiation at the macroscopic scale, which is a critical feature that must be avoided in the design of critical structures. The delaminated sections of some of the specimens (mode II and mode I-II with low mode I ratio) were wedged with a thin-gauged razor blade to eliminate interface friction.

4.1. Mode I

The initial loading was halted after an increment of delamination growth of approximately 3–5 mm. The specimen was then unloaded at a constant displacement rate of 15 mm/min, after which the specimens were again loaded until the final delamination length increment was reached, or the crack extended for at least 25 mm. Modified beam theory (MBT, eq. (4a)), compliance calibration (CC, eq. (4b)), and modified compliance calibration (MCC, eq. (4c)) methods were used to analyze mode I fractures. The corrected energy release rate is expressed as

$$G_I^{MBT} = \frac{3P}{2b(a+\Delta)}\frac{F}{N}\ \text{(a)} \qquad G_I^{CC} = \frac{kP\delta}{2ba}\ \text{(b)} \qquad G_I^{MCC} = \frac{3P^2C^{2/3}}{2A_1bah}\ \text{(c)} \tag{4}$$

where P is the measured load, δ is the load point deflection, C is the compliance, k is the slope of a least-square linear fit of log(C) versus log (a), A_1 is the slope of the MCC curve, and Δ is the correction for the delamination length obtained as the x-intercept of the linear least-squares fit of the cube root of the compliance plotted against the delamination length. F and N are correction factors for large displacements and stiffening effects caused by load-block, respectively [25].

4.2. Mode II

ENF and 4ENF tests were used to characterize initiation and propagation properties as the majority of ENF load deflection responses become unstable after crack initiation. The loading point was perfectly aligned with the loading rollers to minimize the influence of the loading arm on toughness. ENF results are influenced by beam length and the initial delamination, so 4ENF tests were performed to validate the results of the unstable ENF tests. ECM was used to minimize the errors of monitoring and measuring the crack length. The effective crack length and critical energy release rate in ENF-ECM and 4ENF-ECM methods were calculated as follows.

$$r = h\sqrt{\frac{E_1}{72G_{13}}} \tag{5}$$

$$E_1 = \frac{2L^3 + 3(a+r)^3}{8C_{fo}bh^3} \tag{6}$$

$$a_e = \sqrt[3]{\frac{8E_1 b c_f h^3 - 2L^3}{3}} \tag{7}$$

$$G_{IIc} = \frac{9P^2 a_e{}^2}{16b^2 E_1 h^3} \tag{8}$$

$$G_{IIc} = \frac{9P^2(2L-d)^2}{64b^2 E_1 h^3} \tag{9}$$

where effective crack length, a_e, and other parameters for ENF and 4ENF are defined in Table 1 and Fig. 1.

4.3. Mode I-II

It was possible to establish a mixed-mode envelop curve with five sets of data: two pure mode data (modes I and II) and three mixed mode data (different c values). Different ratios of mode I to mode II (0.05, 0.2, and 0.55) were considered. When MMB tests were performed on laboratory specimens, the MMB fixture was quite new, so the deflections of the specimens calculated from DIC were found to be very close to the deflection values for the frame's actuator. The expressions for energy release rates G_{Ic} and G_{IIc} in MMB test are

$$\gamma = \frac{1.\,18\sqrt{E_1 E_2}}{G_{13}} \tag{10}$$

$$\lambda = \frac{E_1}{11G_{13}}\left(3 - 2\left(\frac{\gamma}{\gamma+1}\right)^2\right) \tag{11}$$

$$G_{Ic} = \frac{12P^2(3c-L)^2(a_0+\lambda h)^2}{16b^2h^3L^2E_1} \tag{12}$$

$$G_{IIc} = \frac{9P^2(c+L)^2(a_0+0.42\lambda h)^2}{16b^2h^3L^2E_1} \tag{13}$$

5. Results

5.1. Moisture diffusion in fracture specimens

Fig. 2a shows water absorption curve for the laminated composite at room temperature. It is worth noting that for a given exposure time, the increase of temperature from room temperature (23 °C) to 60 °C caused a faster water uptake. The plot shows water uptake increases at the early stage of the absorption followed by a plateau-type behavior corresponding to an equilibrium condition. There are 2 jumps in water uptake prior to one year of exposure, which could be related to water transport through microcracks and fiber-matrix debonding. The water absorption of the composite laminate at one year of exposure is 0.97%, which is less than the 1.4%–2.15% observed for polymer matrix composites in the literature [30–32]. This can be attributed to the geometry of biaxial stitch-bonded composite, which has continuous fibers and relatively high fiber content in both directions, exhibiting fiber dominated behavior in 0° and a pseudo fiber dominated behavior in 90°. Table 3 summarizes the moisture calculation and compares the Fickian model with the measurements. The Fickian model converges to the measured moisture after one year. The pseudo-equilibrium stage at the end of the plot was extended to obtain water absorption after two years of exposure. If no major non-Fickian jumps occur after the first year, water absorption of 1.21% could be assumed after two years of exposure. Plasticization of the epoxy resin by absorbed moisture was observed in the true stress – true strain curve. This effect caused a reduction in the glass transition temperature and a corresponding degradation of the matrix dominated properties of the composite. Whether or not the free and bound water remained inside the cured composite systems was not a topic of examination for this study. However, Fig. 2b illustrated that after a period of 50 days, there was almost no moisture at the mid-plane of the composite, and consequently

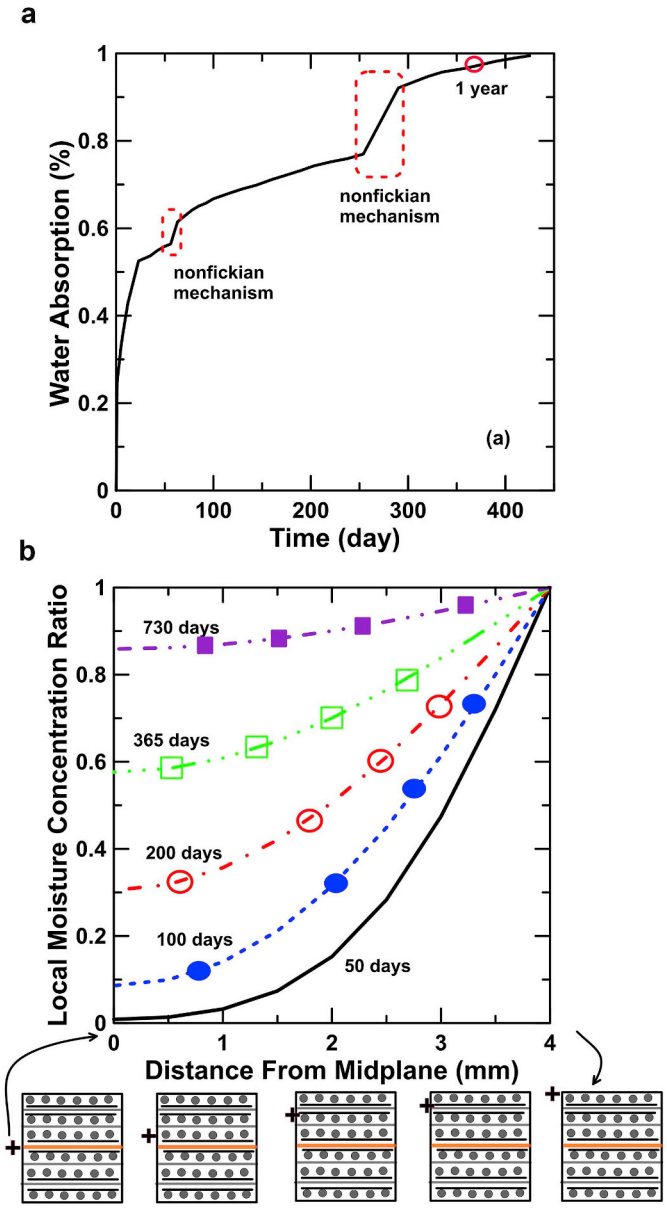

Fig. 2. (a) Percent water absorption due to moisture pickup vs. soaking time for CFRP composite; (b) Moisture profile through the thickness. (For interpretation of the references to color in this figure legend, the reader is referred to the Web version of this article.)

Table 3
Comparison of Fickian weight percent moisture with water absorption measurements.

Time (days)	Moisture concentration ratio (M/M_m)	Measured moisture	Saturated moisture (predicted)	Fickian calculated moisture
50	0.28	0.56%	2%	
100	0.39	0.67%	1.7%	0.79%
200	0.56	0.74%	1.33%	0.95%
365	0.73	*0.97%*	1.33%	*0.97%*
730	0.91			1.21%

no degradation of mechanical and thermophysical properties is expected. However, after one and two years, the level of moisture at the mid-plane is approximately 58% and 86% of the moisture level at the surface of the composite, with the glass transition temperature in hot/

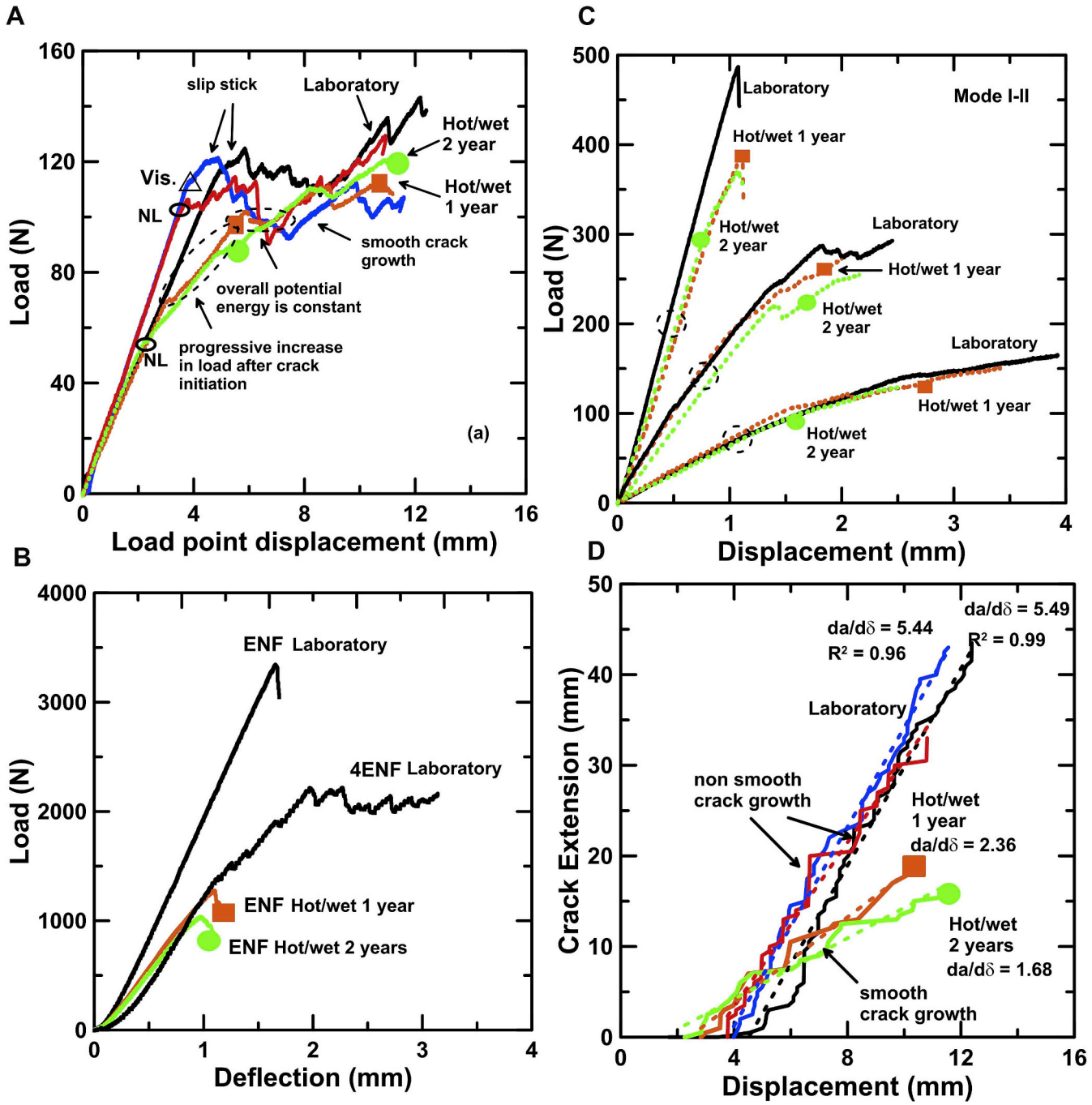

Fig. 3. (a,b,c) Load vs. displacement curve for laboratory and hot/wet conditioned specimens for modes I, II, and I-II; (d) Crack extension vs. load point displacement in mode I for laboratory and hot/wet specimens. (▮: hot/wet 1 year exposure; •: hot/wet 2 years exposure). (For interpretation of the references to color in this figure legend, the reader is referred to the Web version of this article.)

wet conditions after one and two years being 80.8 °C and 78.9 °C, respectively speaking for both moisture and glass transition temperature. A decrease of T_g due to hygrothermal aging was also observed by Belec et al. [29].

5.2. Effects of heat and humidity on load vs. load point displacement of fracture specimens

Representative curves for load versus load-point displacement responses are shown in Fig. 3a,b,3c and are quite different for laboratory and conditioned specimens. For mode I, the load carrying capacity in hot/wet conditioned specimens is reduced by nearly 15% compared to the reference test. These specimens show an increase in load following the initial damage; nevertheless, the post peak behaviors between one- and two-year exposed specimens deviated slightly. The drops in load displacement curves were associated with jumps in crack growth behavior in composite specimens as shown in Fig. 3d; both quasi-static and dynamic crack growth were observed. The crack velocities changed with propagation. In laboratory laminates, the ratio of crack differential to load-point displacement differential (da/dδ) for quasi-static crack behavior was around 4.45, while it was approximately 2.36 for one-year and 1.68 for two-year hot/wet conditioned laminates, respectively.

Fig. 3a indicates that the load in laboratory specimens increased after early crack propagation and before the crack reaches its final

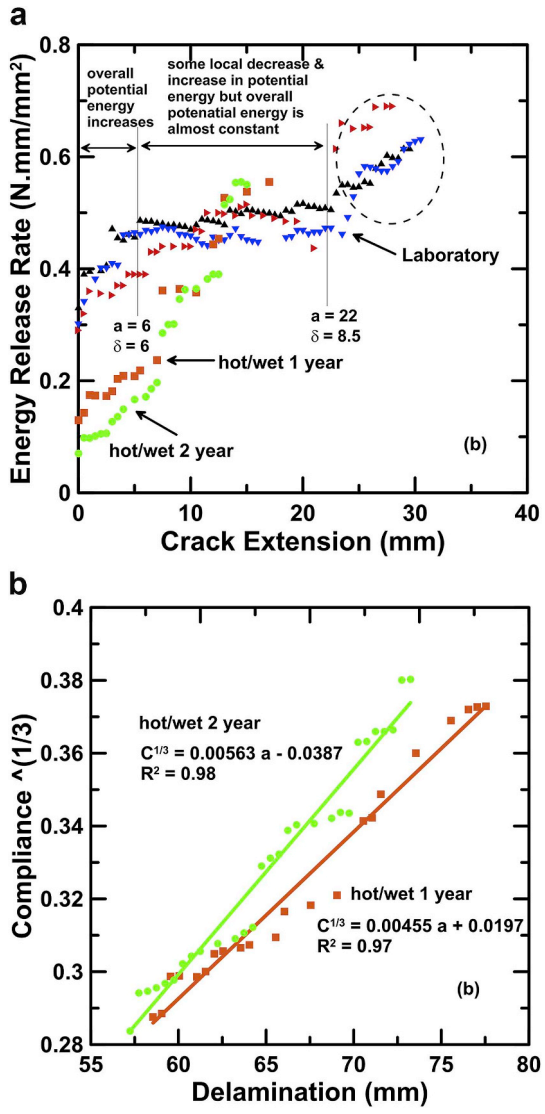

Fig. 4. (a) Mode I energy release rate for laboratory and hot/wet samples; (b) Compliance to the power of one third vs. delamination for 1- and 2-year exposure to hot/wet conditioned samples with the MBT method. (For interpretation of the references to color in this figure legend, the reader is referred to the Web version of this article.)

delamination length. The increase in load enhances the energy release rate at the last stages of crack propagation (extension more than 22 mm) as shown in Fig. 4a (circled area). Markatos [22] attributed this behavior to specimen rotation, as the distance between the crack tip and loading axes increases. Our study showed no rotation or out-of-plane Z direction deformation occurred in the final stages of crack propagation, therefore contrary to Markatos' suggestion, the higher load cannot be attributed to experimental setup misalignment. The differences in the nature of stick-slip behavior could be attributed to variations in composite properties such as resin or fiber-rich regions, misalignment of the fibers in the mid-layers adjacent to the crack plane, voids and other local deviations in microstructure at the central plane of the laminate in front of the crack.

For mode II, the ENF specimens were relatively short with crack length to half span ratio of 0.6 (less than 0.7 recommended by [37]), so load deflection showed unstable crack growth behavior (Fig. 3b). Thermal and humidity degradation correlated with large decreases in the maximum load by 65% for one year, and 70% for two years of exposure. This significant degradation is likely due to the oxidized layer with reduced cohesion at the delamination layer. For mode I-II, a smaller mode I to mode II ratio shows unstable crack growth due to the dominating effect of mode II. The response of a larger mode I to mode II ratio was similar to the response of pure mode I as shown in Fig. 3c. With the exception of mode II, there was no significant difference in initial stiffness between laboratory samples and hot/wet conditioned samples. Unlike the hot/wet samples, the extension of the delamination crack in laboratory specimens was the only fracture mode in the laminates.

6. Discussion

For crack propagation, the competition between fracture and plasticity is influenced by the relation between the Proportional Elastic limit stress (σ_{PEL}) and the Ultimate Tensile Strength (σ_{ULT}). In laboratory specimens, these stresses are very nearly identical, resulting in little plasticity as the crack propagates. In hot/wet conditioned specimens, the mid-layer is degraded and σ_{PEL} is much lower than σ_{ULT}, and as a result, the energy absorption capacity of the interlaminar region and mid-layer is increased as the main crack propagates. Therefore, the propagation energy release rates of the conditioned specimens are not proportional to T_g. The water from hot/wet environmental conditions is typically absorbed by the epoxy resin as 'free' water, and the degradation of mechanical properties of the epoxy resin after a single year of exposure is likely attributed to internal localized residual stresses caused by swelling of the polymer. The specific discussion for each mode of fracture is as follows.

6.1. Mode I

The correction factors Δ were roughly 4.3 and 6.8 mm for the 1- and 2- year exposed samples (Fig. 4b), respectively. A higher value corresponds to larger softening zone, which almost simulates the fracture process zone (FPZ) ahead of the crack tip. It is important to note that a larger softening zone may not substantially affect the initiation energy release rate measured from a sharp pre-crack. The typical strain energy release rate vs. crack growth obtained with the MBT, CC, and MCC methods demonstrate a high degree of correlation among the three methods. Therefore, the strain energy release rate from the MBT method was used for the comparison and development of envelope functions in mixed mode I-II. For all the specimens, the initiation energy release rate was lower than the propagation energy release rate. There were some laboratory specimens which exhibited unstable crack growths during the crack propagation, but the general trend indicated an increase in the energy release rate as the main crack propagated, with a higher slope in the hot/wet conditioned specimens.

The load deflection curves for mode I show that for laboratory specimens, the load increased slightly following crack initiation and dropped locally (instantaneously in most instances, but in some cases gradually) as it passed the point of maximum load. This indicated unstable crack growth behavior. Several load drops and crack jumps were observed in the load vs. load-point deflection and crack extension vs. displacement curves. An R-curve response in laboratory specimens with crack extension of almost 22 mm is shown in Fig. 4a. Davidson and Waas [3] observed the same type of behavior for their energy release rate response, but with milder energy fluctuations for crack propagation. Notably, they studied unidirectional carbon fiber with much thinner fabrics and laminates than what was utilized in our study. Additionally, their loading rate was one order of magnitude higher than the loading rate in this investigation. Unlike laboratory specimens, hot/wet conditioned samples demonstrated much smoother crack propagation with more stable main crack growth behavior. Smooth crack growth behavior was observed by Alessi et al. [32] but Alam Khan et al. [38] showed non-smooth crack growth behavior for hygrothermal conditioned at 70 °C and 85% RH. The epoxy resin carbon fiber composite samples in their work were 3.2 mm thick with a fiber volume fraction of 63% and were conditioned for 64 days. There is no

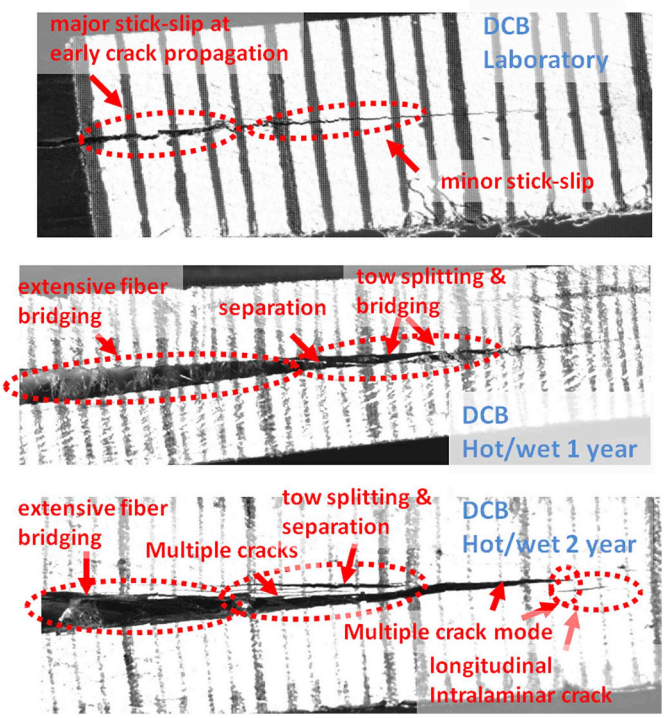

Fig. 5. Different damage modes in laboratory and hot/wet 1- and 2-year for mode I.

information in their paper whether moisture diffused to the mid-plane within the 64 days, and no information on load vs. crosshead displacement of unconditioned specimens was provided either, making an accurate comparison of their results difficult.

Fig. 4a demonstrates that the initiation energy release rate decreases from approximately 0.3 kJ/m^2 for laboratory specimens to 0.15 and 0.13 kJ/m^2 when conditioned for one and two years, respectively. Mohan et al. [24] observed 30% reduction in G_{Ic} when PMCs were conditioned at 98% RH for almost a year. In laboratory samples, the crack propagated within the 0° mid-layer in mode I and mode I-II (with small mode II participation ratio). As the main crack propagated in the hot/wet conditioned samples at the mid-plane, micro-cracks developed at the degraded mid-layers and formed multi-plane intralaminar cracks. These cracks may propagate independently from the main interlaminar crack and may finally merge with the interlaminar crack prior to failure (Fig. 5). Whether the longitudinal intralaminar energy release rate is lower than the interlaminar energy is questionable, however it seems that this might be the reason for observing multiple multi-plane intralaminar cracks. Morais et al. [4] used finite element modeling to show that the intralaminar G is about 30% lower than the interlaminar G in carbon epoxy composites made from carbon T300 toughened epoxy 977–2 prepreg. While there is no consensus on how much intralaminar toughness can be lower than interlaminar, it seems that severe mid-layer degradation in hot/wet specimens (Fig. 5) causes multiple damage modes after crack initiation. Local moisture distribution in Fig. 2b proves high levels of moisture diffused to mid-layers after one year of exposure. In mode I, crack propagation in the mid-layers in the form of longitudinal intralaminar fracture, tow splitting, and separation promoted substantial fiber bridging as shown in Fig. 5, leading to the artificially inflated toughness values in Fig. 4b. The G_{Ic} for hot/wet specimens was almost 3.5 to 4 times the initiation energy release rate; the observed increase in the energy release rate is because of the energy required for the initiation of other damage modes, which cannot be attributed to the real mode I propagation energy release rate.

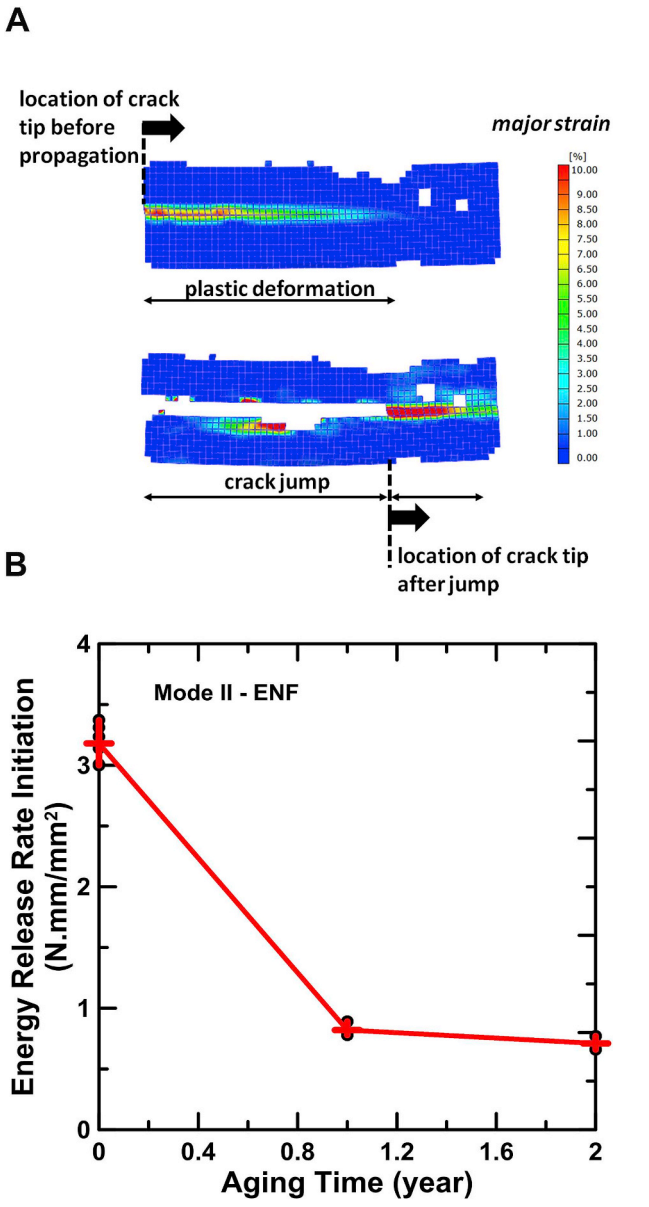

Fig. 6. (a) Unstable crack growth in mode II ENF for hot/wet 1 year; (b) Energy release rate vs. aging time for mode II. (For interpretation of the references to color in this figure legend, the reader is referred to the Web version of this article.)

6.2. Mode II

The ENF results (Fig. 3b) show load drops at the onset of crack propagation for laboratory and hot/wet conditioned samples due to unstable crack growth during ENF testing. The sudden drop in the peak load was associated with the substantial reduction in plastic deformation (Fig. 6a), resulting in a larger distance between the crack tip and support line (left support in the ENF test). This behavior is indicative of unstable crack growth. There was a significant reduction in the mode II energy release rate as humidity increased in the samples as shown in Fig. 2b. The scatter of toughness data in Table 4 was nearly identical for ENF and 4ENF results due to our use of ECM and DIC techniques, whereas Schuecker and Davidson [7] observed a large scatter in ENF results. In Table 4, the classic values refer to toughness computed with a nominal starter crack.

Table 4
Mode II energy release rate.

Sample		ENF (N.mm/mm^2)		4ENF (N.mm/mm^2)
		classic	ECM	ECM
laboratory	avg.	3.06	3.18	3.31
	std.	0.19	0.16	0.15
hot/wet 1 year exposure	avg.	0.78	0.82	–
	std.	0.08	0.05	–
hot/wet 2 years exposure	avg.	0.69	0.71	–
	std.	0.08	0.06	–

Results of the 4ENF tests showed that apart from localized stick-slip behavior, the load increased at the early stages of crack propagation and remained almost constant, implying a nonexistent R curve. Due to the limited number of hot/wet specimens, no tests were conducted using a 4ENF setup, and propagation curves were not calculated for laboratory specimens. Fig. 6b shows that most of the reduction in the mode II fracture energy release rate due to degradation occurs in the first year of exposure to heat and humidity. Less fiber bridging occurred with ENF specimens, compared to DCB specimens-a trend that was also observed by other researchers [14]. Choosing appropriate dimensions for specimens and fixtures in 4ENF tests was complicated due to the complex influence of nonlinearity effects, friction, and compliance on toughness. Schuecker and Davidson [7] and Morais and Pereira [11] showed that a friction coefficient of 0.35–0.5 can be expected in unidirectional polymer carbon composites, which can overestimate G_{IIc} obtained from 4ENF by up to 9%. In our study, due to the small span length and roller diameter in the 4ENF setup, and negating fixture compliance in the energy calculations, the G_{IIc} obtained from 4ENF tests was in good agreement with the energy release rate within 4% from ENF tests. Table 4 shows that the initiation G_{IIc} computed from a nominal starter crack was 3.6% and 5% lower than the true values for laboratory and hot/wet conditioned specimens, respectively. The underestimation in initiation toughness is due to mild nonlinearity and micro-cracks which occur prior to macroscopic crack development.

After fracture tests, the specimens were manually broken apart to investigate the failure modes. Fig. 7 shows the fracture surface for mode II in the region in which the fracture test was conducted. No clear major difference was observed among laboratory and hot/wet specimens. A dull whitish area was observed in each figure followed by shiny black area. The shiny black area is very small in the two-year exposure specimens; it is likely a product of the post mortem inspection as a result of splitting open the specimens. The fracture surfaces in mode II were relatively flat for all the specimens. A small layer of adhesive remained on the surface of the carbon fiber in all the specimens, but it seemed that a more significant amount of adhesive remained on the substrate after 2 years of exposure.

Results of the moisture profile in Fig. 2 showed that the local moisture concentration ratio at the interlaminar region after 2 years (0.86) is much higher than after 1 year (0.58). Since the samples were stored in hot/wet conditions for a relatively long period of time (2 years), it seems that some deleterious effects of the moisture were reversed due to possible increase in the level of bound water. More plasticization, greater level of plastic deformation, and more ductility of the adhesive were expected from 2-year conditioned specimens. The contact at the interlaminar surface in hot/wet specimens is compressed but still a non-bonded connection, termed a kissing bond by Nagy [39]. It seems that the hygrothermal degradation of the energy release rate is somehow proportional to T_g although some limited interfacial fracture mode was observed on the fracture surfaces. The weak kissing bond is extremely crucial to the safety of the composite structure over service life and can be a source of crack initiation during service life if not appropriately considered during structural design.

6.3. Mode I-II

Fig. 8a shows the interaction between G_{Ic} and G_{IIc} in MMB test setup, showing that G_{II} decreased as G_I increased and both G_{Ic} and G_{IIc} decreased with exposure to hot/wet conditions. The high 0.96 correlation coefficient validated the regression polynomial curve as the envelop function. A linear function (dashed line) was added as a reference to show that for the most part, the interaction between modes was on the weaker side. Stronger interaction between the modes exists when the fracture mode changes from pure mode I or II to mixed mode for all the specimens. The interaction curve based on $G = G_I + G_{II}$ was also examined for the dataset as shown in Fig. 8b-this type of curve does not show the interaction for low values of G_{II}, particularly for hot/wet specimens. Based on this, the interaction curve based on G is not recommended as a reference for brittle thermoset resins with low G_I and high G_{II} values (averaged $G_I = 0.08$ kJ/m^2 and $G_{II} = 0.71$ kJ/m^2). The locus may change as the crack grows, particularly in the hot/wet conditioned specimens, as mid-layer degradation significantly influences crack propagation as expected from Fig. 9. In our study, small- and large-scale fiber bridging were distinguished between laboratory and hot/wet conditioned specimens in mode I-II with a high mode I ratio

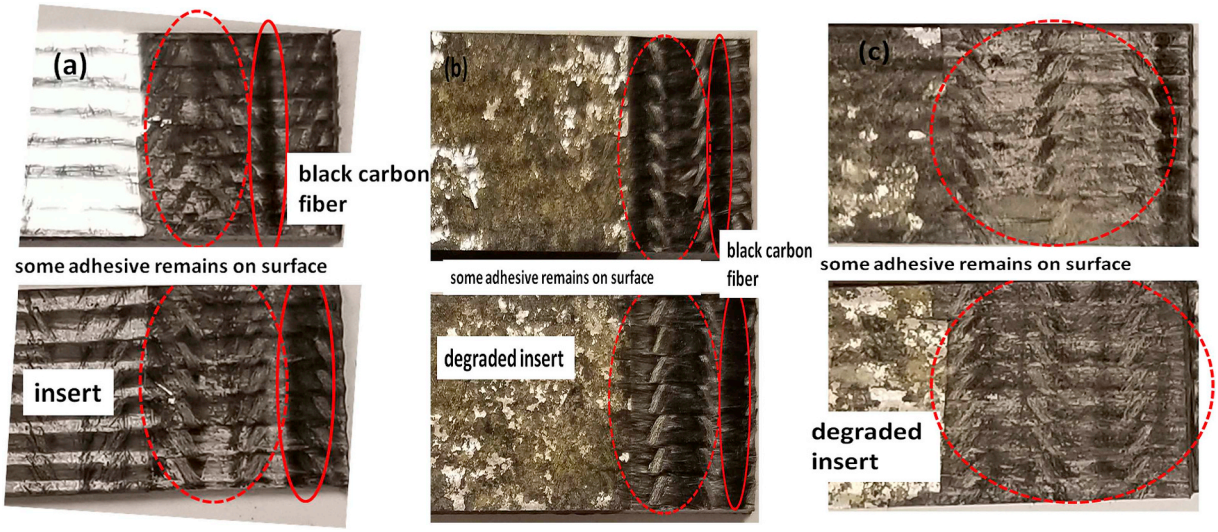

Fig. 7. Typical fracture surfaces for mode II (a) laboratory condition, and (b,c) hot/wet condition for 1 and 2 year exposure, respectively. The crack propagation was from left to right. (For interpretation of the references to color in this figure legend, the reader is referred to the Web version of this article.)

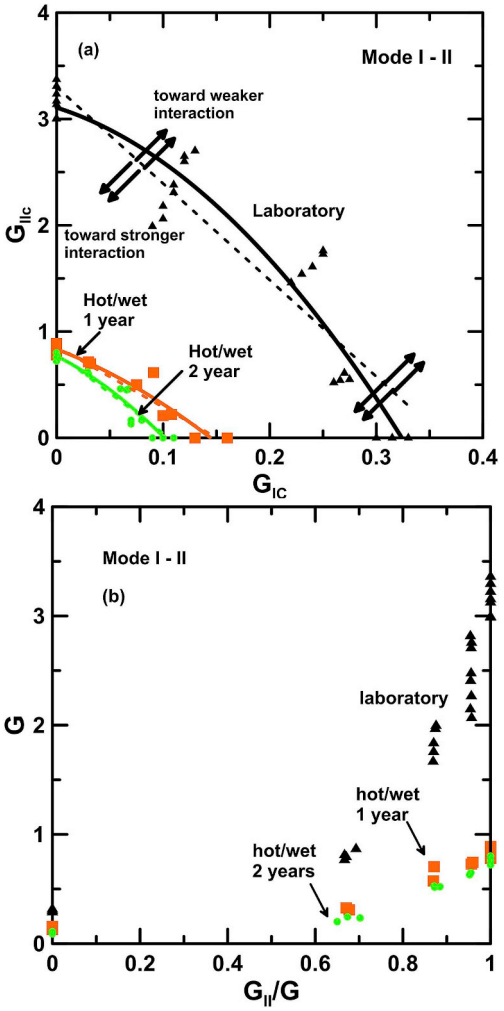

Fig. 8. Envelope functions in mixed mode fractures for laboratory and hot/wet conditioned specimens.

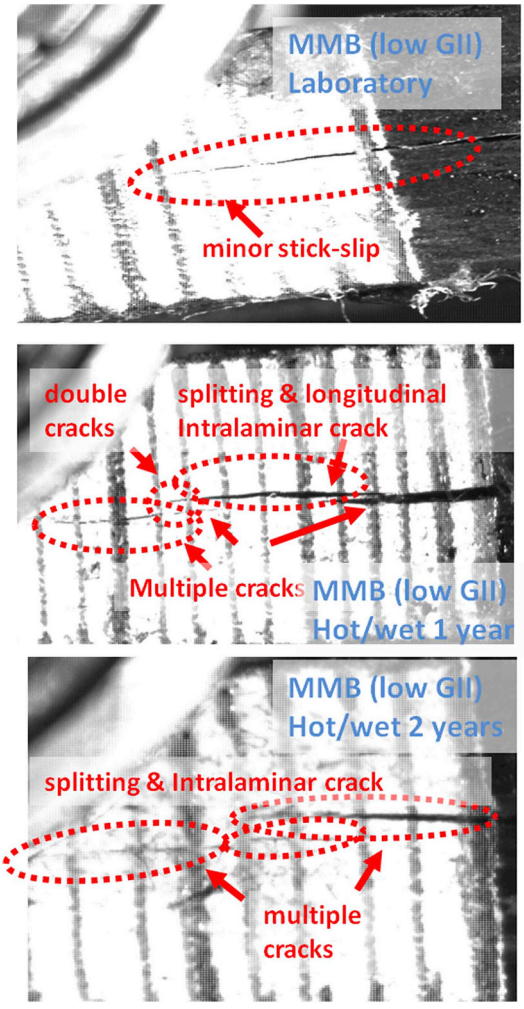

Fig. 9. Different damage modes for laboratory and hot/wet 1- and 2- year mode I-II fracture with low G_{II}. (For interpretation of the references to color in this figure legend, the reader is referred to the Web version of this article.)

and in mode I fracture (Figs. 5 and 9). In the latter case, the fiber bridging spanned along nearly the entire length of the specimen behind the crack tip. No data is available on the possible R curve effect for the hot/wet specimens due to complexities of multiple crack propagations.

Experiments performed on specimens without the wedge in mode II and mode I-II showed that removing the wedge did not affect the load displacement curves. A very small difference in the magnitude of 3.5% was observed in the calculation of G_{II} initiation between wedged and un-wedged unidirectional carbon fiber composites by Landry et al. [40]. In aged samples of mode I and mode I-II with low mode II participation ratio, as the crack initiated under displacement control mode, the driving energy dropped below the threshold value of the main interlaminar crack. As a result, the load increased, and the newly stored elastic energy caused the formation of macroscopic cracks as intralaminar fractures located in the mid-layers. These cracks grow while the main interlaminar crack is either stationary or grows with much lower crack speed compared to unaged specimens. Fig. 10 illustrates bare broken fibers on SEM inspections of the fracture surfaces evidencing a dense fiber bridging and smooth crack propagation of one and two year hot/wet specimens in mode I-II fracture with large G_I participation. The SEM images indicate a mixture of adhesive and cohesive fracture proving the failure takes place in a mix of ductile matrix and the weakened fiber/matrix interface. Fig. 10 also shows a relatively thinner-layer cohesive failure in two-year hot/wet specimen proving that the failure surface is very close to the adhesive-substrate interface. However, comparison of the fiber/resin adhesion between one and two year hot/wet specimens shows no further degradation. The physics of the transitions among multiple cracks is not yet well understood and is under consideration as the focus of future research.

7. Conclusion

Polymer matrix composite fracture during service life for modes I, II, and mixed I-II fracture were studied. There was a dramatic reduction in initiation energy release rate for all the fracture modes due to exposure to elevated temperature (60 °C) and high levels of humidity (90%). Energy release rate in mode I fracture reduced by 50% in one-year and two-years hot/wet conditioned specimens. Crack branching and deviation from the central plane invalidated the toughness results for mode I crack propagation in hot/wet specimens. The mode II initiation fracture properties resulted in a much larger reduction in initiation energy rate, showing a rate of 70% for the hot/wet conditioned specimens. The initiation energy release rates for all fracture modes, particularly for mode II, are proportional to the glass transition temperature of the epoxy resin. The reduction in the initiation energy release rate for all the fracture modes is due to moisture diffusion to the mid-layer. The glass transition temperature reduced with the exposure of samples to hot/wet conditions.

The effective crack method (ECM) approach was used to compute crack length and toughness in mode II. Application of ECM and a Digital Image Correlation (DIC) system reduced the errors in calculation of

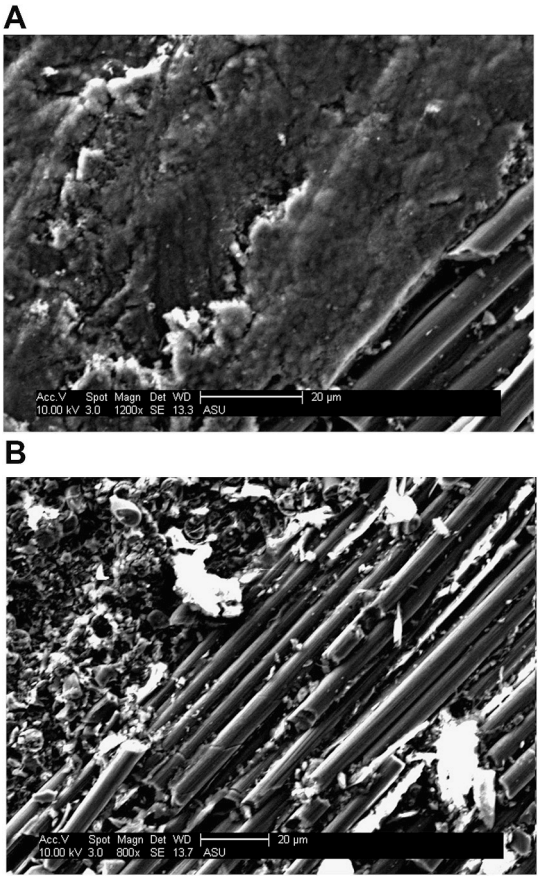

Fig. 10. SEM image of fracture surface under mode I-II with high G_I participation for hot/wet conditioned sample (a) 1 year exposure; (b) 2 year exposure.

energy due to extra compliance and crack positioning. The G_{IIc} initiation as obtained from ENF and 4ENF tests for laboratory and hot/wet conditioned specimens are in good agreement and demonstrated that the difference between ENF and 4ENF results is negligible if deflection and crack lengths are accurately measured and the specimen and fixture geometry are chosen appropriately.

Multiple intralaminar and interlaminar damage modes, crack branching and deviation from the central plane, and significant fiber bridging were observed during propagation in mode I and mixed mode I-II, with a low mode II participation ratio for hot/wet conditioned specimens. The mechanisms of energy absorption due to plasticity and energy distribution among multiple cracks for inter- and intralaminar crack modes during propagation are unknown. Therefore, delamination resistance can only be quantified for crack initiation in hot/wet conditioned specimens. Both quasi-static and dynamic fracture mode behaviors exist in mode I and mixed mode, with a low level of mode II participation, particularly in laboratory specimens. The transition between these modes is stochastic in nature and is dependent on some macro- and microscopic characterizations such as initial crack length, resin/fiber rich zones in front of the crack tip, and voids. SEM of the fracture surfaces of one- and two-year hot/wet specimens showed large number of fibers appear clean with areas of fiber covered with epoxy resin. The small difference between energy release rates after one year and two years can be attributed to the relatively long conditioning time and the possible increase in 'bound' water content in the material. The results also indicate that G_{II} decreases as G_I increases for all the specimens. Most interactions between the modes are weak; however, stronger interaction exists when the fracture mode changes from a pure mode to a mixed mode.

Data availability

The raw/processed data required to reproduce these findings cannot be shared at this time as the data also forms part of an ongoing study.

Acknowledgments

This research was supported by Pipe Reconstruction Inc. (grant no. FP00004034).

Appendix A. Supplementary data

Supplementary data to this article can be found online at https://doi.org/10.1016/j.polymertesting.2019.05.010.

References

[1] M.J. Mathews, S.R. Swanson, Characterization of the interlaminar fracture toughness of a laminated carbon/epoxy composite, Compos. Sci. Technol. 67 (2007) 1489–1498.
[2] T. Kusaka, M. Hojo, Y.W. Mai, T. Kurokawa, T. Nojima, S. Ochiai, Rate dependence of mode I fracture behavior in carbon fiber epoxy composite laminates, Compos. Sci. Technol. 58 (5) (1998) 91–602.
[3] P. Davidson, A.M. Waas, Non-smooth mode I fracture of fiber-reinforced composites: an experimental, numerical and analytical study, Phil. Trans. R. Soc. 370 (2012) 1942–1965.
[4] A.B. Morais, M.F. De Moura, A.T. Marques, A.T. Castro, Mode I interlaminar fracture of carbon/epoxy cross ply composites, Compos. Sci. Technol. 62 (2002) 679–686.
[5] C.R. Corleto, W.L. Bradley, Mode II Delamination Fracture Toughness of Unidirectional Graphite/epoxy Laminates, ASTM STP., 1989, pp. 201–221.
[6] W. Wang, T. Vu-Khanh, Use of the end-loaded split (ELS) test to study stable fracture behavior of composites under mode II loading, Compos. Struct. 36 (1996) 71–79.
[7] C. Schuecker, B.D. Davidson, Evaluation of the accuracy of the four-point bend end-notched flexure test for mode II delamination toughness determination, Compos. Sci. Technol. 60 (2000) 2137–2146.
[8] S. Hashemi, A.J. Kinloch, J.G. Williams, The effects of geometry, rate and temperature on the mode I, mode II and mixed-mode I/II interlaminar fracture of carbon fiber/poly (ether-ether ketone) composites, J. Compos. Mater. 24 (1990) 918–956.
[9] M.F.S.F. De Moura, A.B. De Morais, Equivalent crack based analyses of ENF and ELS tests, Eng. Fract. Mech. 75 (2008) 2584–2596.
[10] R.H. Martin, B.D. Davidson, Mode II fracture toughness evaluation using a four point bend end notched flexure test, Plast., Rubber Compos. 28 (8) (1992) 401–406.
[11] A.B. De Morais, A.B. Pereira, Application of the effective crack method to mode I and mode II interlaminar fracture of carbon/epoxy unidirectional laminates, Compos. Part A 38 (2007) 785–794.
[12] J.R. Reeder ., J.H. Crews, Mixed mode bending method for delamination testing, AIAA J. 28 (1990) 1270–1276.
[13] J.R. Reeder ., J.H. Crews Jr., Redesign of the mixed-mode bending delamination test to reduce nonlinear effects, J. Compos. Technol. Res. 14 (1992) 12–19.
[14] S. Hashemi, A.J. Kinloch, G. Williams, Mixed-mode fracture in fiber polymer composite laminates", in: T.K. O'Brien (Ed.), Composite Materials: Fatigue and Fracture, vol. 1110, ASTM STP, 1991, pp. 143–168.
[15] A.J. Russell, K.N. Street, Moisture and temperature effect on the mixed-mode delamination fracture unidirectional graphite/epoxy, in: W.S. Johnson (Ed.), Delamination Debonding of Materials, ASTM, 1985, pp. 349–370.
[16] J.R. Reeder ., A bilinear failure criterion for mixed-mode delamination, in: E.T. CamponechiJr. (Ed.), Composite Materials: Testing and Design, vol. 1206, ASTM STP, 1993, pp. 303–322.
[17] K.Y. Rhee, Characterization of delamination behavior of unidirectional graphite/PEEK laminates using cracked lap shear (CLS) specimens, Compos. Struct. 29 (1994) 379–382.
[18] J.R. Reeder, J.H., Crews Jr., Nonlinear Analysis and Redesign of the Mixed-Mode Bending Delamination Test. NASA Technical Memorandum 102777, (1991).
[19] F. Ducept, P. Davies, D. Gamby, An experimental study to validate tests used to determine mixed-mode failure criteria for glass/epoxy composites, Composer Part A. 28A (1997) 719–729.
[20] A.J. Kinloch, Y. Wang, J.G. Williams, P. Yayla, The mixed-mode delamination of fiber composite materials, Compos. Sci. Technol. 47 (1993) 225–237.
[21] M.L. Benzeggagh, M. Kenane, Measurement of mixed-mode delamination fracture toughness of unidirectional glass/epoxy composites with mixed-mode bending apparatus, Compos. Sci. Technol. 56 (1996) 439–449.
[22] Y. Zhang, A.P. Vassilopoulos, T. Keller, Effects of low and high temperatures on tensile behavior of adhesively-bonded GFRP joints, Compos. Struct. 92 (7) (2010) 1631–1639.
[23] D.N. Markatos, K.I. Tserpes, E. Rau, S. Markus, B. Ehrhart, S. Pantelakis, The effects

of manufacturing and in-service related boding quality reduction on the mode I fracture toughness of composite bonded joints for aeronautical use, Compos. Part B. 45 (1) (2013) 556–564.
[24] J. Mohan, A. Ivakovic, N. Murphy, Mode I fracture toughness of co-cured and secondary bonded composite joints, Int. J. Adhesion Adhes. 51 (2014) 13–22.
[25] J. Mohan, A. Ivakovic, N. Murphy, Effect of prepreg storage humidity on the mixed-mode fracture toughness of a co-cured composite joint, Compos. Part A. 45 (2013) 23–34.
[26] J. Zhou, J.P. Lucas, Hygrothermal effects of epoxy resin. Part I:The nature of water in epoxy, Polymer 40 (1999) 5505–5512.
[27] J. Zhou, J.P. Lucas, Hygrothermal effects of epoxy resin. Part II: variations of glass transition temperatures, Polymer 40 (1999) 5513–5522.
[28] N.G. Berry, J.R.M. dAlmeida, F.L. Barcia, B.G. Soares, Effect of water absorption on the thermomechanical properties of the HTPB modified dgeba-based epoxy systems, Polym. Test. 26 (2007) 262–267.
[29] A. Megueni, A. Tounsi, E. Adda Bedia, Evolution of the stress intensity factor for patched crack with bonded hygrothermal aged composite repair, Mater. Des. 28 (2007) 287–293.
[30] S.J. Hooper, R. Subramanian, 4th, Effects of Water and Jet Fuel Absorption on Mode I and Mode II Delamination of Graphite/epoxy. Composite Materials: Fatigue and Fracture vol. 1156, ASTM, 1993, pp. 318–340.
[31] L. Belec, T.H. Nguyen, J.F. Chailan, Comparative effects of humid tropical weathering and artificial ageing on a model composite properties from nano- to macro-scale, Comp. Part A. 68 (2015) 235–241.
[32] S. Alessi, G. Pitarresi, Spadaro. Effect of hydrothermal ageing on the thermal and delamination fracture CFRP composites, Comp. Part B. 67 (2014) 45–55.
[33] C.H. Shen, G.S. Springer, Moisture absorption desorption of composite materials, J. Compos. Mater. 10 (2014) 2–20.
[34] AC. Loos, GS. Springer. Moisture absorption of graphite/epoxy composites immersed in liquids and in humid air. In Springer, G. S. ed., Environmental Effects on Composite Materials, p. 34-50.
[35] R. DeIasi, JB. Whiteside. Effect of moisture on epoxy resins and composites. In Vinson, J. R. ed., Advanced Composite Materials – Environmental Effects, ASTM STP vol. 658, 2-20. Philadelphia, PA.
[36] CE. Browning, GE. Husman, JM. Whitney. Moisture effects in epoxy matrix composites. Composite Materials: Testing and Design: 4th Conference , ASTM STP vol. 617, 481-496. Philadelphia, PA.
[37] L.A. Carlsson, J.W. Gillespie JR, R.B. Pipes, On the analysis and design of the end notch flexure (ENF) specimen for mode II testing, J. Comput. Math. 20 (1986) 594–604.
[38] L. Alam Khan, A.H. Mahmood, A.S. Syed, Z.M. Khan, R.J. Day, Effect of hygro-thermal conditioning on the fracture toughness of carbon/epoxy composites cured in autoclave/Quickstep, J. Reinf. Plast. Compos. 32 (2013) 1165–1176.
[39] P.B. Nagy, Ultrasonic detection of kissing bonds at adhesive interfaces, Adhes. Sci. Technol. 5 (8) (1991) 619–630.
[40] B. Landry, G. LaPlante, L.R. LeBlanc, Environmental effects on mode II fatigue delamination growth in an aerospace grade carbon/epoxy composite, Compos. Part A. 43 (2012) 475–485.